Decadal warming of coastal China Seas and coupling with winter monsoon and currents

L.-Y. Oey,[1,2] M.-C. Chang,[1] Y.-L. Chang,[3] Y.-C. Lin,[1] and F.-H. Xu[4]

Received 3 October 2013; revised 15 November 2013; accepted 18 November 2013; published 4 December 2013.

[1] In recent decades, wintertime sea surface temperatures off the eastern coast of China have steadily increased. The warming is accompanied by on-coast wind convergence across East China Sea and by stronger northeasterly wind which is spatially inhomogeneous being greatest in the Taiwan Strait. Strong winds favor more frequent cross-shelf currents and vigorous spreading of heat from the Kuroshio, which warms the coastal sea in a positive feedback loop. The process also weakens the East Asian winter monsoon over eastern China, contributing to its decoupling from the recent rebound of the Siberian High. **Citation:** Oey, L.-Y., M.-C. Chang, Y.-L. Chang, Y.-C. Lin, and F.-H. Xu (2013), Decadal warming of coastal China Seas and coupling with winter monsoon and currents, *Geophys. Res. Lett.*, *40*, 6288–6292, doi:10.1002/2013GL058202.

1. Introduction

[2] The world's ocean has warmed most notably in the last three decades; the warming is believed to be caused by radiative imbalance of the atmosphere due to increased greenhouse gases [*Trenberth et al*., 2007; *Hansen et al*., 2010], with the ocean absorbing most of the heat [*Bindoff et al*., 2007]. Increased ocean heat content began from late 1970s to early 1980s [*Rayner et al*., 2006], and a steep warming followed shortly after the 1997–1998 El Niño [*Balmaseda et al*., 2013]. Simultaneously, studies have reported a large-scale weakening of the East Asian winter monsoon (EAWM) and the Siberian High since the 1970s, which has been attributed to climate warming [e.g., *Panagiotopoulos et al*., 2005; *Xu et al*., 2006; *Lee et al*., 2013].

[3] Because of their proximity to land and other unique regional factors, the coastal seas are generally subject to greater temperature changes than the open ocean [*Belkin*, 2009]. In winter (January, February, March (JFM)) off the eastern coast of China, *Lima and Wethey* [2012, their Figure 6] found a warming trend of ~1°C/decade, compared to the global mean sea surface temperature (SST) rise of ~0.13°C/decade [*Trenberth et al*., 2007]. The strong warming may impact the monsoon wind, which in turn may alter the ocean currents, hence the distribution of heat, in a coupled manner. How do the atmosphere and ocean respond to the strong warming, and how are the responses related to the large-scale EAWM? Quantifying and explaining the coupled changes in winter monsoon wind, SST and currents in East China Sea (ECS) during the recent decades is the goal of this study.

2. Data

[4] High-resolution (1/4° × 1/4° gridded) daily SST from 1982 to 2012 [*Reynolds and Chelton*, 2010] and 6-hourly cross-calibrated multiplatform (CCMP) [*Atlas et al*., 2011] wind from 1988 to 2009 are used to compute linear trends, long-term (~10 years) averages, and other statistics. The SST data were used by *Lima and Wethey* [2012]; we follow their methods (their p. 11) which include the removal of pixels with more than 50% of land contamination. The CCMP is an extensively validated product which combines European Centre for Medium-Range Weather Forecasts (ECMWF) reanalysis with satellite surface winds and winds from ships and buoys [*Atlas et al*., 2011]; on land, the ECMWF surface winds are used. Unless indicated otherwise, seasonal climatological values are removed from time series, and quoted correlations and trends are based on the 95% significance. Currents obtained from the North Pacific Ocean model of *Oey et al*. [2013a] at 0.1° × 0.1° resolution, and 41 levels are used to infer long-term trends of cross-shelf flows. The model is forced by the CCMP wind from 2 July 1987 to 31 December 2009. Details are reported in *Oey et al*. [2013a].

3. Wind and SST Rise

[5] In Taiwan Strait, the seasonal amplitude of the northeasterly wind stress (rotated 30° clockwise from north) increased especially after the 1997–1998 El Niño (Figure 1a). The wind became more intense showing an overall trend of generally increasing speed of about 2–3 m s^{-1} from 1988 to 2009 (Figure 1b). However, during the first decade of the record from 1988 to 1998, the speed was generally decreasing, which agrees with *Xu et al*. [2006] and *Hung and Kao* [2010], who attributed the decrease to the weakening trend of the EAWM since ~1970. The trend became generally increasing from 1998 to 2009, which seems to be consistent with the large-scale rebound of the EAWM reported by *Jeong et al*. [2011].

[6] To understand how the increasing northeasterly wind in Taiwan Strait after 1998 may be related to the large-scale EAWM, we compare trends for the period before and after 1998 over China and northwest Pacific (Figures 2a and 2b) and plot also the whole record (1988–2009) trend over a larger domain that includes northern Mongolia and part of central Siberia (40–60°N, 105–125°E; Figure 2c). From 1988 to 1998, southwesterly trend prevailed in ECS and

Additional supporting information may be found in the online version of this article.

[1]Institute of Hydrological & Oceanic Sciences, National Central University, Jhongli, Taiwan.
[2]Program in Atmospheric & Oceanic Sciences, Princeton University, Princeton, New Jersey, USA.
[3]Institute of Marine Environmental Science and Technology, National Taiwan Normal University, Taipei, Taiwan.
[4]Ministry of Education Key Laboratory for Earth System Modeling, and Center for Earth System Science, Tsinghua University, Beijing, China.

Corresponding author: L.-Y. Oey, National Central University, No. 300, Zhongda Rd., Jhongli, Taoyuan County 320, Taiwan. (lyo@princeton.edu)

0094-8276/13/10.1002/2013GL058202

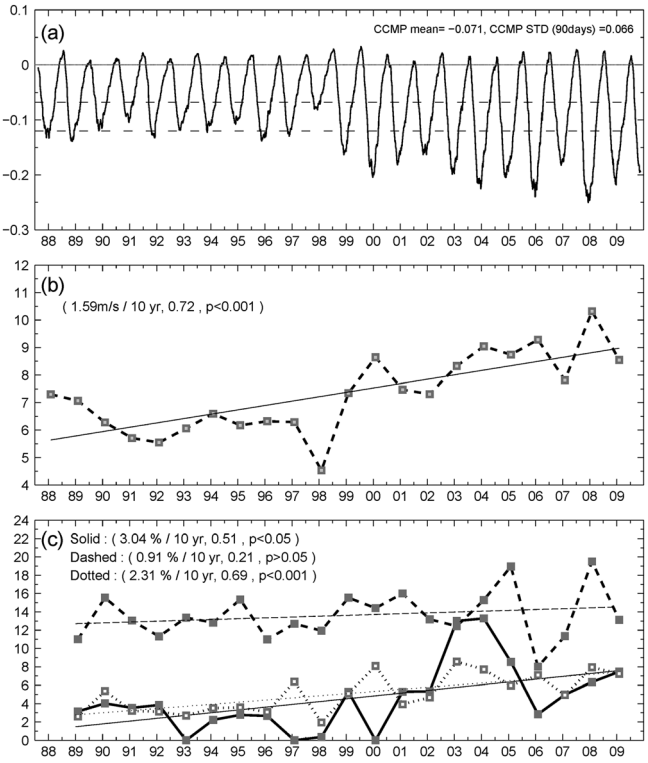

Figure 1. (a) Along-strait wind stress ($\mathrm{N\,m^{-2}}$; 90 day running mean) using drag formula of *Oey et al*. [2006] in Taiwan Strait, positive northeastward. Dashed lines are -0.12 and $-0.068\,\mathrm{N\,m^{-2}}$ (supporting information). Mean and standard deviation are shown in top right. (b) JFM wind speed ($\mathrm{m\,s^{-1}}$) and (c) $C_{\mathrm{ccc,twn}}$ and $C_{\mathrm{tws,twn}}$ (solid and dashed lines) in % and average of $C_{\mathrm{twn,ccc}}$ and $C_{\mathrm{tws,ccc}}$ (dotted line) for 21 winters 1989–2009. The three values in parentheses across top in Figures 1b and 1c are trend, correlation, and p-value. The "$p < 0.05$" indicates trend is significant at the 95% confidence level, etc. Trends of $C_{\mathrm{twn,ccc}}$ and $C_{\mathrm{tws,ccc}}$ separately are 2.1%/10 year and 2.5%/10 year, respectively, with $C_{\mathrm{tws,ccc}}$ showing more contrast before (less) and after (more) 1998.

across central China. After 1998, northeasterly trend prevailed over the shelves and slopes of the southern ECS and northern South China Sea, as well as portions of central China. Since the EAWM is anticyclonic (Figure 2d, red vectors), the northeasterly wind became generally weaker from 1988 to 1998 and stronger from 1998 to 2009. However, the trend was not spatially uniform and was strongest over the southern ECS and in the Taiwan Strait. The Siberian High has rebounded as seen in the increasing trend of the whole record (Figure 2c) in the region 40–60° N and 105–125°E, in agreements with *Jeong et al*. [2011]. The large-scale rebound extended east into Korea and Japan but was separated from the positive trends over the shelf seas by a cyclonic trend over China: negative trends over central and eastern provinces of China and positive trends over southwestern China. This complex overland pattern resembles the observations during the weakening phase of the EAWM [*Niu et al*., 2010, their Figure 3b; *Lee et al*., 2013, their Figure 3].

[7] The increasing trend of northeasterly wind over shelf seas and its separation from rebound of the Siberian High by complex cyclonic trend over China suggest a regional dynamics which may be related to coastal SST warming. Figure 2d shows an overlay of the differences in wind (black vectors and contours) and SST (color) between the periods before and after 1998. The averaging period for SST is 1 year ahead of that for the wind, anticipating the lag between them, shown below. The SST difference shows that the ocean has warmed 0.2–2°C after 1998 compared to the decade before. The warming was part of the overall global warming in which coastal SST increased at a faster rate than global [*Belkin*, 2009; *Lima and Wethey*, 2012]. However, preferentially strong warming of 1–2°C existed from the southern shelf of the ECS into the Taiwan Strait. Coincident with this local SST rise is stronger wind speeds which in the vicinity of the Taiwan Strait are as much as $+3\,\mathrm{m\,s^{-1}}$. The decadal increase in wind speed in the Taiwan Strait is likely related to SST warming. Warmer sea produces more vigorous turbulence in the planetary boundary layer, which brings faster moving air from aloft, accelerating the wind near the sea surface [*Wallace et al*., 1989]. However, the maximum wind speed difference is slightly downwind of the maximum SST difference.

[8] We use empirical orthogonal functions (EOFs) [*Kutzbach*, 1967] to understand the connection between SST and wind (Figure 3). Mode-1 SST (Figures 3a and 3b, color) explains 52% of the variance; its principle component PC1(SST) shows a decadal rise from 1982 to 2010 with transition near 1997–1998. The rise occurred preferentially during JFM winter (the 360 day running mean PC1 (not shown) follows closely the JFM PC1) and was dominated by heterogeneous warming of the shelf seas as clearly seen in the eigenvector EV1(SST) (Figure 3a). The shelf seas including the Taiwan Strait experienced 4–5 times stronger SST warming than the open ocean. Modes 1 and 2 (not shown) of the wind velocity ($\boldsymbol{u}_w$) explain 50% and 21% of the total variance; their PC1 and PC2 are interannual and generally out of phase with El Niño-Southern Oscillation (ENSO) [e.g., *Zhang et al*., 1997]. Of interest here are modes 3 and 4 (Figure 3a, black vectors (mode 3 only); Figure 3c, vectors; and Figure 3d) which explain 8% and 6.5%, respectively, of the total variance, and which like mode-1 SST are dominated by wintertime decadal rise in their PCs with sign changes near 1998–2000. They are barely separable but are distinct from neighboring modes 2 and 5 according to the criterion of *North et al*. [1982]; following *Zhang and Hendon* [1997, p.744], we interpret them together as one pattern. Both PCs correlate with the wind (correlation coefficients $\approx$ 0.7). The PC4 slightly leads PC3, but both lag the PC1 (SST) by 1–2 years (see caption). Concomitant with warming over the shelf seas, the spatial pattern is cyclonic centered northwest of Taiwan (Figures 3a and 3c), consisting of east-southeasterly on-shelf flow north of the cyclone, represented by EV3($\boldsymbol{u}_w$), and north-northwesterly offshore flow south of the cyclone, represented by EV4($\boldsymbol{u}_w$). The pattern is consistent with Figure 2d that over the outer shelf of the ECS the differenced wind (black vectors) veers onshore compared to the mean wind (red vectors) and suggests a thermally driven, low-level wind convergence into the warm shelf. The warm coastal seas therefore act as a sink of low-level wind which accelerates as it turns cyclonically into the strait channeled by the high mountains of Taiwan; this may explain why the maximum speed is downwind of the warming (Figure 2d). Moreover, since cyclonic wind anomaly

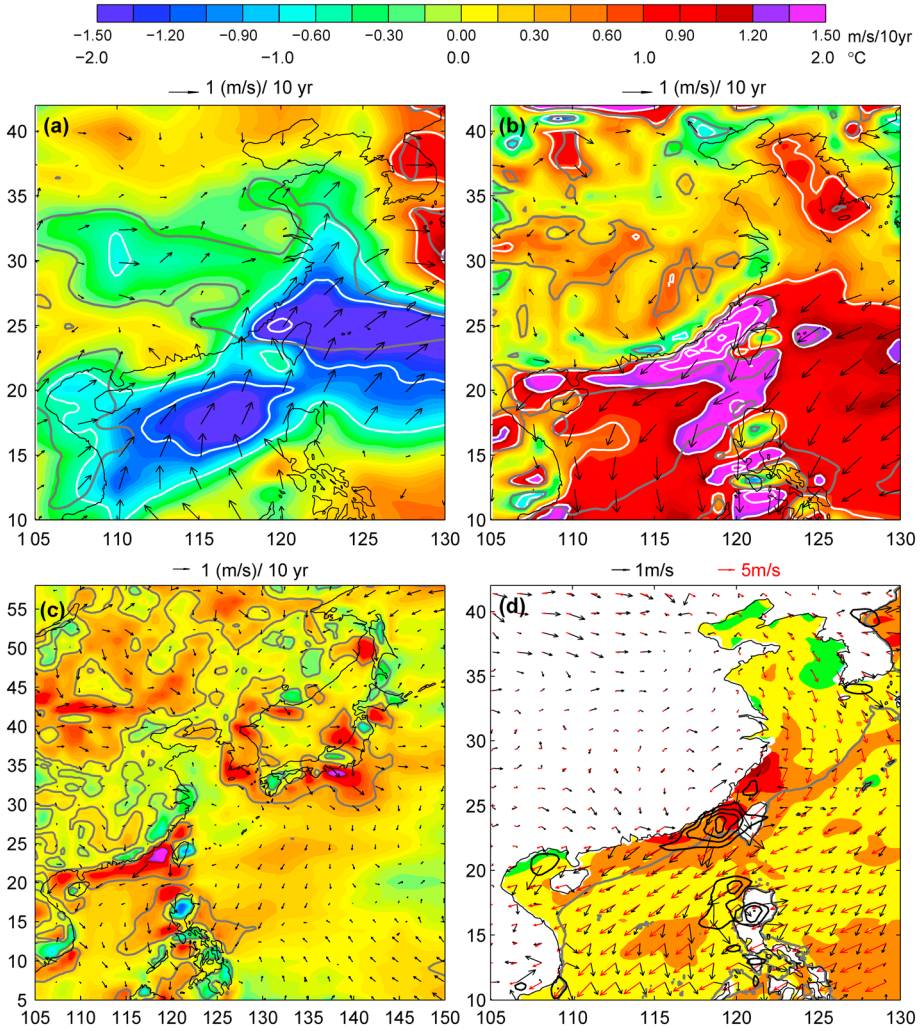

Figure 2. Winter (mean JFM) trends in wind speed (color and white contours −1.8, −1.2, −0.6, 0.6, 1.2, … 3 m s^{-1} per decade) and vectors (with lengths limited to 1 m s^{-1} per decade for clarity), for (a) 1988–1998 and (b) 1998–2009; grey contour is $p = 0.05$. (c) Same but for whole record (1988–2009) and larger region (white contours omitted). (d) Wind difference (1999–2009 JFM minus 1988–1998 JFM) black vectors and speed contours from 1.5 m s^{-1} at interval = 0.5 m s^{-1}, superimposed on SST difference (color in °C; 1998–2009 JFM minus 1987–1997 JFM). Red vectors are 1988–2009 JFM-mean wind (note different scale as shown on top). Grey contour is the 200 m isobath.

with scales ~1000 km generally prevails west-northwest of the heating [*Gill*, 1980], the SST warming might possibly explain the cyclonic trend pattern over China and contributed to the weakening trend of the northeasterly wind over the eastern provinces of China (Figure 2c) where EV4($\boldsymbol{u}_w$) dominates (Figure 3c). *Chang and Oey* [2013] found a similar cyclonic trend induced by SST warming off the coast of Venezuela.

4. Ocean Currents

[9] What is the heat source of the coastal warming, and why is the SST rise localized near the Taiwan Strait (Figures 2d, 3a, and 3b)? Given the large atmospheric scales, the phenomenon is likely related to ocean variability. *Belkin* [2009, his Figure 4] found strong summer warming off the Yangtze River (32°N, 122°E) and suggested that solar heat is preferentially trapped in the stratified layer of the plume. In winter, stratification is weak [e.g., *Li et al*., 2006]. An alternative explanation is that heat from Kuroshio is transported across shelf to the coast, but such a transport is not obvious given that the tendency of coastal flow is along shelf [*Allen*, 1980]. Assuming barotropic dynamics, *Oey et al*. [2013b; see supporting information] show the existence of two critical wind stress values (Figure 1a) such that currents in Taiwan Strait are predominantly equatorward (poleward) for strong (weak) winds, with little cross-shelf transports. For moderate or relaxing winds, we follow *Oey et al*. [2013b] and composite the model currents for the 21 winters from 1988 to 2009 (Figure 3a, white vectors). These show a cyclone in the northern Taiwan Strait and cross flows into the two regions of preferred warming: in the midstrait and along the China coast from 26° to 28°N, separated by a relative SST minimum that coincides with the cyclone downstream of the ridge. Physics of the cross flows are explained in *Oey et al*. [2013b] where references of relevant observations are given.

[10] Averaged over many events, cross flows produce a net heat transport toward China, and since they tend to develop as sufficiently strong northeasterly monsoon relaxes, a higher frequency of them would accompany the decadal strengthening

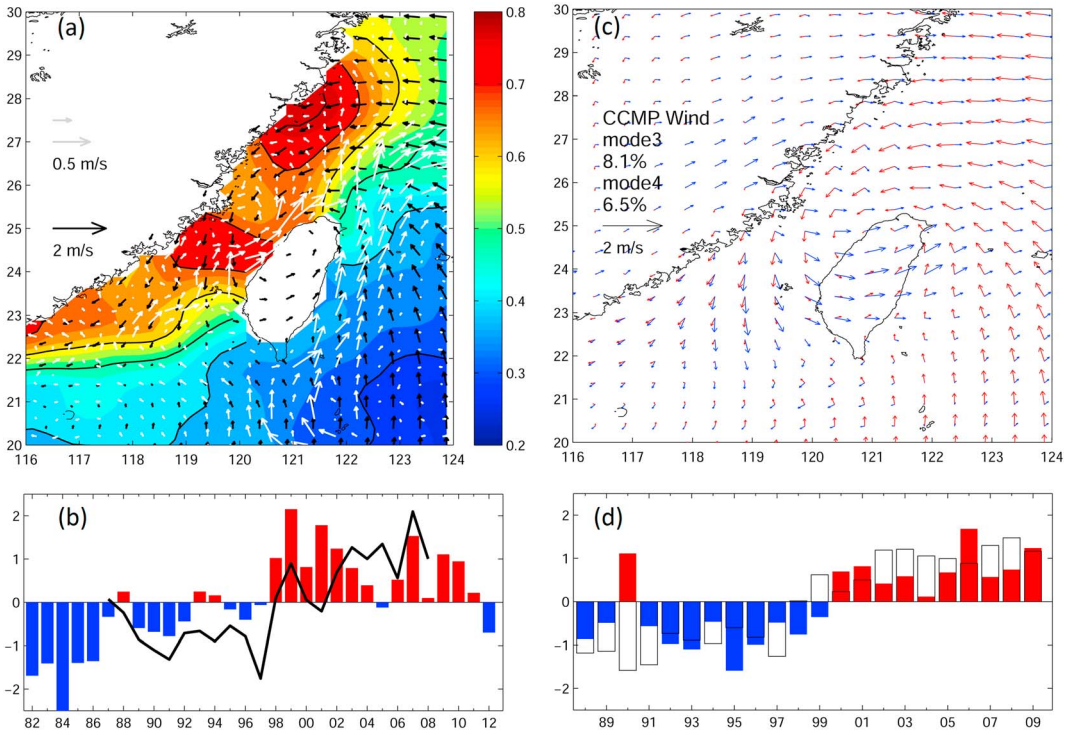

Figure 3. Mode-1 EOF(SST) (a) EV1 (CI = 0.2°C) with EV3($\boldsymbol{u}_w$) (black vectors and scale) and composite ocean current (see text; white vectors in two scales on shelf (bigger) and open seas), and (b) JFM-mean PC1(SST) for the period 1982–2012, and back line is annual wind speed (m s^{-1}) from Figure 1b shifted to the left by 1 year (i.e., wind lags) when correlation Corr(PC1 (SST),$|\boldsymbol{u}_w|$) is maximum ≈ 0.6. (c) EV3($\boldsymbol{u}_w$) (red) and EV4($\boldsymbol{u}_w$) (blue) and (d) their corresponding JFM-mean PC3 (color bars) and PC4 (open bars). Here PC1(SST) leads PC4($\boldsymbol{u}_w$) by about 1 year, which in turn leads PC3($\boldsymbol{u}_w$) by another 1 year. The corresponding maximum correlations are Corr(PC1(SST), PC4($\boldsymbol{u}_w$), +1 year) ≈ 0.7 and Corr(PC1(SST), PC3($\boldsymbol{u}_w$),+2 years) ≈ 0.63, all significant at the 95% significance level.

of the northeasterly monsoon. Winds also force onshore Ekman transport of warm Kuroshio water northeast of Taiwan [*Chang et al.*, 2010]. To identify cross-shelf spreading of heat from waters of different origins and then quantify long-term trends of these processes, 120 particles are released biweekly from each of the four coastal zones along China and Taiwan for each winter of 1988–2009, from 1 December to 15 March of the following year. The zones are each 30 km wide across shore and are denoted as SCC: South China Coast south of 24°N; CCC: Central China Coast from 24 to 28°N; TWS: Taiwan South Coast (south of 24°N along Taiwan west coast); and TWN: Taiwan North Coast (north of 24°N along Taiwan west coast). For each release (eight per winter), particles' positions at $N = 20$ and 30 days, which are roughly the time taken for particles to drift across the shelf, are recorded to calculate the connectivity matrix [*Paris et al.*, 2007]. Each matrix element $C_{i,j}$ is the percent of particles originating from the ith-source and arriving in the jth-target. Thus, $C_{\mathrm{ccc,twn}} = \%$ of particles from CCC arriving in TWN, and vice versa for $C_{\mathrm{twn,ccc}}$; both measure the strength of cross flows. Similarly, $C_{\mathrm{tws,twn}}$ and $C_{\mathrm{tws,ccc}}$ measure the strength of Kuroshio intrusion and spreading toward the Chinese coast, respectively. The mean (and standard deviation) from the 16 (= 8 releases × 2 Ns) samples are calculated for each winter to form 21 year time series shown in Figure 1c below the wind plots. There are interannual changes, some of which appear to be ENSO related, suggesting complex processes. Three of the Cs display increasing trends: 3% per decade for $C_{\mathrm{ccc,twn}}$ for particles transported to Taiwan's northwestern coast from China and approximately 2–2.5% per decade for particles which spread onto the China's central coast from northern Taiwan ($C_{\mathrm{twn,ccc}}$) and from Kuroshio intrusion southwest of Taiwan ($C_{\mathrm{tws,ccc}}$). While the trend of 0.9% for $C_{\mathrm{tws,twn}}$ is not significant, it nonetheless suggests that the supply of warm water due to the Taiwan Warm Current has probably not weakened despite the stronger northeasterly wind. The results in Figure 1c suggest that the frequencies of Kuroshio intrusions and cross flows have likely steadily increased in the past decades, consistent with the idea of a more efficient spreading of heat from the Kuroshio, hence to the observed coastal warming.

5. Discussion

[11] Warmer coastal sea induces low-level cyclonic wind convergence onto the ECS shelf, modulating the convective instability of the atmosphere and in turn may cause increased precipitation. Using the high-resolution Tropical Rainfall Measuring Mission product (http://daac.gsfc.nasa.gov), we find an increasing trend of precipitation in winter of 1999–2013 (not shown) in Taiwan Strait and southern ECS. The trend is consistent with analyses based on large-scale reanalysis data [*Zhang et al.*, 2009]. Onshore wind appears to be consistent also with the more frequent wintertime fog observed in recent decades over eastern China [*Niu et al.*, 2010, their Figures 1 and 2a]. However, strong ENSO-related variations exist [e.g., *Zhou*, 2010]. Longer observational data at high resolution to separate large-scale and local effects are necessary.

[12] Our findings may be of importance to the regional ecosystem. The cold-water copepod species *Calanus sinicus*, for example, drift south along the coast of China in winter but are often observed some 100 km across shelf off the northwestern and northern coasts of Taiwan [*Hwang and Wong*, 2005; *Hwang et al*., 2006]. The distributions of *C*. *sinicus* provide evidence of cross flows [*Oey et al*., 2013b] which may modulate over long time scales, controlling their fates. Ocean currents affect temperature (and salinity) upon which fish depends for their habitat and survival; the long-term coupled changes in SST and monsoon wind here described might therefore be important for the studies of fish species [*Chang et al*., 2004].

6. Conclusion

[13] In recent decades, warming of shelf seas off the eastern coast of China was accompanied by stronger northeasterly wind and by on-shelf wind convergence from the open Pacific. Stronger northeasterly monsoon would favor more frequent intrusions and vigorous spreading of heat from the Kuroshio, which in turn induces warmer coastal seas in a positive feedback loop. Since SST leads the wind, the coupled response might have been triggered by the strong warming of the 1997–1998 El Niño. Finally, the increased northeasterly wind over coastal seas is found to be detached from the recent rebound of the Siberian High by a cyclonic wind trend over China.

[14] **Acknowledgments.** We thank the reviewers for their suggestions to improve the manuscript.

[15] The Editor thanks Igor Belkin and an anonymous reviewer for their assistance in evaluating this paper.

References

Allen, J. S. (1980), Wind-driven currents on continental shelf, *Annu. Rev. Fluid Mech.*, *12*, 389–433.

Atlas, R., R. N. Hoffman, J. Ardizzone, S. M. Leidner, J. C. Jusem, D. K. Smith, and D. Gombos (2011), A cross-calibrated, multiplatform ocean surface wind velocity product for meteorological and oceanographic applications, *Bull. Am. Meteorol. Soc.*, *92*, 157–174.

Balmaseda, M. A., K. E. Trenberth, and E. Källén (2013), Distinctive climate signals in reanalysis of global ocean heat content, *Geophys. Res. Lett.*, *40*, 1754–1759, doi:10.1002/grl.50382.

Belkin, I. M. (2009), Rapid warming of large marine ecosystems, *Prog. Oceanogr.*, *81*, 207–213.

Bindoff, N. L., et al. (2007), Observations: Oceanic climate change and sea level, in *Climate Change: The Physical Science Basis*, pp. 385–432, Cambridge Univ. Press, New York.

Chang, C.-W., S.-H. Lin, Y. Iizuka, and W.-N. Tzeng (2004), Relationship between Sr:Ca ratios in Otoliths of grey mullet Mugil cephalus and ambient salinity: validation, mechanisms, and applications, *Zool. Stud.*, *43*(1), 74–85.

Chang, Y.-L., and L.-Y. Oey (2013), Coupled response of the trade wind, SST gradient, and SST in the Caribbean Sea, *J. Phys. Oceanogr.*, *43*, 1325–1344.

Chang, Y.-L., L.-Y. Oey, C.-R. Wu, and H.-F. Lu (2010), Why are there upwellings on the northern shelf of Taiwan under northeasterly winds?, *J. Phys. Oceanogr.*, *40*, 1405–1417.

Gill, A. E. (1980), Some simple solutions for heat-induced tropical circulation, *Q. J. R. Meteorol. Soc.*, *106*, 447–462.

Hansen, J., R. Ruedy, M. Sato, and K. Lo (2010), Global surface temperature change, *Rev. Geophys.*, *48*, RG4004, doi:10.1029/2010RG000345.

Hung, C.-W., and P.-K. Kao (2010), Weakening of the winter monsoon and increase of winter rainfalls over northern Taiwan and southern China in early 1980s, *J. Clim.*, *23*, 2357–2367.

Hwang, J.-S., and C. K. Wong (2005), The China Coastal Current as a driving force for transporting Calanus sinicus, *J. Plankton Res.*, *27*, 205–210.

Hwang, J.-S., et al. (2006), A 5-year study of the influence of the northeast and southwest monsoons on copepod in East China Sea and the Taiwan Strait, *J. Plankton Res.*, *28*, 943–958.

Jeong, J.-H., T. Ou, H. W. Linderholm, B.-M. Kim, S.-J. Kim, J.-S. Kug, and D. Chen (2011), Recent recovery of the Siberian High intensity, *J. Geophys. Res.*, *116*, D23102, doi:10.1029/2011JD015904.

Kutzbach, J. (1967), Empirical eigenvectors of sea level pressure, surface temperature, and precipitation complexes over North America, *J. Appl. Meteorol.*, *6*, 791–802.

Lee, S.-S., S.-H. Kim, J.-G. Jhun, K.-J. Ha, and Y.-W. Seo (2013), Robust warming over the East Asia during the boreal winter monsoon and its possible causes, *Environ. Res. Lett.*, *8*, 034001, doi:10.1088/1748-9326/8/3/034001.

Li, C., J. Hu, S. Jan, Z. Wei, G. Fang, and Q. Zheng (2006), Winter-spring fronts in Taiwan Strait, *J. Geophys. Res.*, *111*, C11S13, doi:10.1029/2005JC003203.

Lima, F. P., and D. S. Wethey (2012), Three decades of high-resolution coastal sea surface temperatures reveal more than warming, *Nat. Commun.*, *3*, 704.

Niu, F., Z. Li, C. Li, K.-H. Lee, and M. Wang (2010), Increase of wintertime fog in China: Potential impacts of weakening of the Eastern Asian monsoon circulation, *J. Geophys. Res.*, *115*, D00K20, doi:10.1029/2009JD013484.

North, G. R., T. L. Bell, and R. F. Cahalan (1982), Sampling errors in the estimation of empirical orthogonal functions, *Mon. Weather Rev.*, *110*, 699–706.

Oey, L.-Y., T. Ezer, D.-P. Wang, S.-J. Fan, and X.-Q. Yin (2006), Loop current warming by Hurricane Wilma, *Geophys. Res. Lett.*, *33*, L08613, doi:10.1029/2006GL025873.

Oey, L.-Y., Y.-L. Chang, Y.-C. Lin, M.-C. Chang, F. Xu, and H.-F. Lu (2013a), ATOP—The Advanced Taiwan Ocean Prediction System based on the mpiPOM: Model descriptions, analyses and results, *Terr. Atmos. Ocean. Sci.*, *24*, 137–158.

Oey, L.-Y., Y.-L. Chang, Y.-C. Lin, M.-C. Chang, S. Varlamov, and Y. Miyazawa 2013b, Cross flows in the Taiwan Strait in winter. *J. Phys. Oceanogr.* (http://journals.ametsoc.org/doi/abs/10.1175/JPO-D-13-0128.1), in press.

Panagiotopoulos, F., M. Shahgedanova, A. Hannachi, and D. B. Stephenson (2005), Observed trends and teleconnections of the Siberian High: A recently declining center of action, *J. Clim.*, *18*(9), 1411–1422, doi:10.1175/JCLI3352.

Paris, C. B., L. M. Cherubin, and R. K. Cowen (2007), Surfing, spinning, or diving from reef to reef: Effects on population connectivity, *Mar. Ecol. Prog. Ser.*, *347*, 285–300.

Rayner, N. A., P. Brohan, D. E. Parker, C. K. Folland, J. J. Kennedy, M. Vanicek, T. J. Ansell, and S. F. B. Tett (2006), Improved analyses of changes and uncertainties in SST measured in situ since the mid-nineteenth century: The HadSST2 dataset, *J. Clim.*, *19*, 446–469.

Reynolds, R. W., and D. B. Chelton (2010), Comparisons of daily sea surface temperature analyses for 2007–08, *J. Clim.*, *23*, 3545–3562.

Trenberth, K. E., et al. (2007), Climate change 2007: The physical science basis, in *Contribution of Working Group I to the Fourth Assessment Report of the Intergovernmental Panel on Climate Change*, edited by S. Solomon et al., *996*, pp. 235–336, Cambridge Univ. Press, Cambridge, U. K., and New York.

Wallace, J. M., T. P. Mitchell, and C. Deser (1989), The influence of SST on surface wind in the eastern equatorial Pacific: Seasonal and interannual variability, *J. Clim.*, *2*, 1492–1499.

Xu, M., C.-P. Chang, C. Fu, Y. Qi, A. Robock, D. Robinson, and H. Zhang (2006), Steady decline of East Asian monsoon winds, 1969–2000: Evidence from direct ground measurements of wind speed, *J. Geophys. Res.*, *111*, D24111, doi:10.1029/2006JD007337.

Zhang, C., and H. H. Hendon (1997), Propagating and standing components of the intraseasonal oscillation in tropical convection, *J. Atmos. Sci.*, *54*, 741–752.

Zhang, Y., K. R. Sperber, and J. S. Boyle (1997), Climatology and interannual variation of the EAWM: Results from the 1979–95 NCEP/NCAR reanalysis, *Mon. Weather Rev.*, *125*, 2605–2619.

Zhang, Z., D. Gong, M. Hu, D. Guo, X. He, and Y. Lei (2009), Anomalous winter temperature and precipitation events in southern China, *J. Geogr. Sci.*, *19*, 471–488.

Zhou, L.-T. (2010), Impact of EAWM on rainfall over SE China and its dynamical processes, *Int. J. Climatol.*, *31*, 677–686, doi:10.1002/joc.2101.